J. Fluid Mech. (2010), *vol.* 647, *pp.* 53–69. © Cambridge University Press 2010
doi:10.1017/S0022112009993752

Intrusive gravity currents between two stably stratified fluids

BENJAMIN D. MAURER,[1] DIOGO T. BOLSTER[2] AND P. F. LINDEN[3]†

[1]Scripps Institution of Oceanography, La Jolla, CA 92093-0208, USA

[2]Department of Civil Engineering and Geological Sciences, University of Notre Dame, IN 46556, USA

[3]Department of Mechanical and Aerospace Engineering, University of California, San Diego, La Jolla, CA 92093-0411, USA

(Received 14 September 2009; revised 24 November 2009; accepted 1 December 2009)

We present an experimental and numerical study of one stratified fluid propagating into another. The two fluids are initially at rest in a horizontal channel and are separated by a vertical gate which is removed to start the flow. We consider the case in which the two fluids have the same mean densities but have different, constant, non-zero buoyancy frequencies. In this case the fluid with the smaller buoyancy frequency flows into the other fluid along the mid-depth of the channel in the form of an intrusion and two counter-flowing gravity currents of the fluid with the larger buoyancy frequency flow along the top and bottom boundaries of the channel. Working from the available potential energy of the system and measurements of the intrusion thickness, we develop an energy model to describe the speed of the intrusion in terms of the ratio of the two buoyancy frequencies. We examine the role of the stratification within the intrusion and the two gravity currents, and show that this stratification plays an important role in the internal structure of the flow, but has only a secondary effect on the speeds of the exchange flows.

1. Introduction

Intrusions or intrusive gravity currents occur when horizontal density gradients result in the intrusion of one fluid into another fluid at an intermediate depth. Intrusions are closely related to gravity currents which occur when one fluid flows into another of different density along a horizontal boundary (Simpson 1997). The presence of vertical density stratification of the receiving fluid is a necessary condition for the existence of an intrusion, and the literature (e.g. Amen & Maxworthy 1980; Faust & Plate 1984; Ungarish 2005; Bolster, Hang & Linden 2008; Nokes *et al.* 2008) has traditionally investigated gravity currents and intrusions containing fluid of uniform density into a stratified ambient fluid. However, in many natural and industrial flows the intruding fluid is also stratified and the role of this stratification and its influence on the exchange flow are the subject of this paper.

For the case of an unstratified intrusion, the potential energy stored in the intrusion relative to the surrounding ambient fluid is converted into the kinetic energy of

† Email address for correspondence: pflinden@ucsd.edu

https://doi.org/10.1017/S0022112009993752 Published online by Cambridge University Press

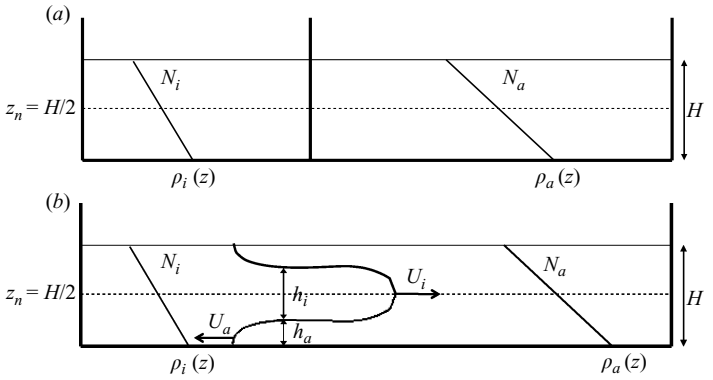


FIGURE 1. Schematic showing the initial conditions of lock release of a linearly stratified intruding fluid of constant buoyancy frequency N_i, into a linearly stratified ambient fluid of buoyancy frequency N_a, where the average densities of both fluids are equal. When the barrier is removed, the intrusion propagates along the level of neutral buoyancy $z_n = H/2$ at a speed that is a function of the stratification ratio $S = N_i^2/N_a^2$.

horizontal motion. This motion has been shown to be important to the transport of mass, energy, and particulate matter in environmental flows, from dust storms and seafloor turbidity currents to locust and plankton distributions (Simpson 1997). The intruding fluid carries material with it, and an unstratified intrusion has relatively little internal circulation and any internal flow is traditionally ignored in the analysis of the flow (Lowe, Linden & Rottman 2002). For example, Benjamin's (1968) classical analysis of a gravity current assumes that the current moves as a plug with an equal forward velocity at all points in the current.

When the intruding fluid itself is stratified, there is the added possibility of vorticity being generated within the intrusion itself by the interaction of the pressure gradients and the density gradients—the so-called baroclinic generation of vorticity. This internal circulation can be significant depending on the magnitude of the stratification within the intrusion. This work aims to extend our understanding of high Reynolds number, Boussinesq intrusive gravity currents to the case in which stratification exists in *both* the ambient and the intruding fluids.

Intrusive gravity currents are often studied in the context of lock-release experiments, in which a finite volume of fluid is released into a larger body of stratified fluid by the rapid removal of a vertical barrier (e.g. Keulegan 1958; Amen & Maxworthy 1980). We consider the case in which the fluids on both sides of the barrier have the same depth H, their densities are linear functions of height, $\rho(z) = \rho(z_n) + (\rho_0/g)N^2 z$, and their average densities $\rho_i(z_n) = \rho_a(z_n)$ are the same. Here z_n is the level of neutral buoyancy chosen to be the mid-depth of the channel for both fluids, ρ_0 is a reference density, g is gravity and $N = \sqrt{-(g/\rho_0)(\partial\rho/\partial z)}$ is the buoyancy frequency of the stratification, and the subscripts i and a refer to the intruding and ambient fluids, respectively, and by definition $N_i < N_a$ (figure 1). When the barrier is removed at $t = 0$, the intrusion flows into the ambient fluid along the level of neutral buoyancy at the mid-depth of the ambient fluid, while two gravity currents of ambient fluid travel in the opposite direction, one along the upper and the other along the lower boundaries of the tank. The choice of linear stratification and equal mean densities means that the flow is vertically symmetric about the mid-depth of the

https://doi.org/10.1017/S0022112009993752 Published online by Cambridge University Press

tank. If this condition is relaxed then the fluid with the lower centre of gravity would tend to flow beneath the other producing a bulk circulation within the flow field.

In this case, after a brief period of acceleration, the intrusion travels into the ambient fluid at a constant speed for multiple lock lengths before decelerating, similar to observations by Maxworthy *et al.* (2002) of well-mixed boundary currents in a stratified ambient fluid. We limit our study to this initial constant-velocity phase of propagation, during which the lock fluid is unaffected by the presence of the endwall of the lock. At later times we expect the finite volume of the lock to become important and, at these times an unstratified intrusion decelerates. This is the so-called similarity phase (Rottman & Simpson 1983). Although we expect similar behaviour to occur for a stratified intrusion, it has not been considered in this work.

For an unstratified ($N_i = 0$) mid-depth intrusion into a linearly stratified ambient fluid, dimensional analysis implies that, at high Reynolds numbers, the intrusion speed U_i during the initial constant velocity phase takes the form

$$U_i = F N_a H, \tag{1.1}$$

where F is a dimensionless Froude number. Treating the midplane intrusion as two symmetric well-mixed boundary gravity currents reflected about the midplane of the tank, Bolster *et al.* (2008) extended findings of Maxworthy *et al.* (2002) and Ungarish (2005) to show that $F \approx 0.125$. Bolster *et al.* (2008) also show that, during this initial constant-velocity phase of propagation, (1.1) is consistent with the constant rate of conversion of available potential energy to kinetic energy, and that such energy conversion also predicts the speed of intrusions that are not located at the mid-depth of the tank. Here, we extend the energy conversion model for mid-depth intrusions to incorporate the role of stratification in the intruding fluid, $N_i > 0$, and examine the effect of the consequent reduction in the available potential energy on the speed of the intrusion during the constant-velocity phase.

In § 2 we present the mathematical model, which in this case needs to take account of the varying intrusion thickness with N_i, and a prediction of the intrusion speed. We describe laboratory experiments and two-dimensional numerical simulations in § 3 and compare the results with the theory in § 4. In §§ 5 and 6, we compare our results with those of the unstratified case and discuss the role of the stratification within the intrusion.

2. Model

Following the approach of Cheong, Kuenen & Linden (2006) and Bolster *et al.* (2008), we consider an energy model relating the conversion of available potential energy of the initial hydrostatic pressure imbalance before the lock is opened to the constant increase of kinetic energy in the current after the gate is removed.

The lock release can be described in terms of two dimensionless parameters: the Froude number F defined by (1.1) and the stratification ratio S of the intruding and ambient fluid stratifications

$$S \equiv N_i^2 / N_a^2, \tag{2.1}$$

where, by definition, $0 \leqslant S \leqslant 1$. When $S = 0$, the intruding fluid is well-mixed and corresponds to the case described by Bolster *et al.* (2008), where the intrusion travels at

$$U_i(S = 0) \approx 0.125 N_a H. \tag{2.2}$$

https://doi.org/10.1017/S0022112009993752 Published online by Cambridge University Press

When $S=1$, $N_i^2=N_a^2$, the densities of the two fluids on either side of the lock are identical and, obviously,

$$U_i(S=1)=0. \tag{2.3}$$

A dimensional analysis implies that

$$U_i = 0.125 N_a H f(S), \tag{2.4}$$

where the factor of 0.125 is to account for the value of the Froude number for unstratified intrusions $S=0$, and the dimensionless function $f(S)$ of the stratification ratio S must satisfy the criteria imposed by (2.2) and (2.3) that $f(0)=1$ and $f(1)=0$.

In order to determine the form of $f(S)$, we examine the available potential energy (APE) as a function of the stratification ratio. Taking the level of neutral buoyancy as the reference level, the APE per unit volume is

$$E = g\int_{-H/2}^{H/2}(\rho_i-\rho_a)z\,\mathrm{d}z, \tag{2.5a}$$

$$= \frac{gH^2}{6}(\rho_a-\rho_i)|_{-h/2}, \tag{2.5b}$$

$$= \frac{\rho_0 H^3 N_a^2}{12}(1-S). \tag{2.5c}$$

We normalize E by the available potential energy $(1/12)\rho_0 H^3 N_a^2$ of a well-mixed intrusion (Bolster *et al.* 2008). This leads to a non-dimensional form E^* of the APE per unit volume in terms of the stratification ratio S

$$E^* = (1-S). \tag{2.6}$$

As the simplest extension of the analysis of an unstratified intrusion (Bolster *et al.* 2008), we first neglect the motion in the counterflowing gravity currents and assume that the intrusion thickness is independent of S. Assuming that the rate of conversion of APE to the intrusion kinetic energy (proportional to U^2) is constant in time, then

$$f(S) \sim (1-S)^{1/2}. \tag{2.7}$$

However, we observe (see § 4) that the thickness of the intrusions varies with S. At high Reynolds number, the thickness h_i of an unstratified intrusion $S=0$ is observed to be approximately one-half the total depth of the fluid, $h_i(S=0)=H/2$. For the case where the buoyancy frequencies of both the intruding fluid and the ambient fluid are equal, the current can be viewed as having a current thickness equal to the full height of the fluid, $h_i(S=1)=H$. For intermediate values of S, the vertical distance between isopycnals in the ambient fluid corresponding to the minimum and maximum densities of the intrusion varies linearly with S. Therefore, as a first approximation, we assume a linear increase in the thickness of the intrusion with S,

$$h_i = \frac{H}{2}(1+S). \tag{2.8}$$

Still ignoring the counterflowing gravity currents, but now relating the kinetic energy of the current to the available potential energy while taking into account the variation of the intrusion thickness with S, we find that

$$f(S) \sim \left(\frac{1-S}{1+S}\right)^{1/2}. \tag{2.9}$$

https://doi.org/10.1017/S0022112009993752 Published online by Cambridge University Press

However, the counterflowing gravity currents above and below the intrusion also carry kinetic energy. In order to account for the energy in the counterflowing currents, we note that (2.8) implies

$$h_a = \frac{H}{2}(1 - S). \tag{2.10}$$

Because there is no net volume flux across a vertical plane, the speed of the counterflows U_a is given by

$$U_a = \frac{h_i}{2h_a}U_i. \tag{2.11}$$

Finally, scaling the kinetic energy of both the forward and backward propagating flows of varying thickness with the APE, we obtain

$$f(S) \sim \frac{(1 - S)}{(1 + S)^{1/2}}. \tag{2.12}$$

The energy scaling models in (2.7), (2.9) and (2.12) will be compared with the results of laboratory experiments and numerical simulations in § 4.

3. Methods

3.1. *Laboratory experiments*

Laboratory experiments were conducted in a channel with an ambient fluid with a fixed stratification $N_a = 1.47 \pm 0.02\ \mathrm{s}^{-1}$, and for six values of the stratification ratio $S = \{0, 0.23, 0.38, 0.49, 0.65, 0.77\}$. The Reynolds number, based on the observed propagation speed and intrusion thickness, of the slowest propagating intrusion ($S = 0.77$) was found to be in excess of 10^3, the value above which unstratified gravity currents are considered inviscid (Simpson 1997).

The experimental channel was 182 cm long, 23 cm wide and 30 cm deep, with a vertical gate dividing the tank at a distance of $L_{lock} = 63$ cm from an endwall. Removing the gate vertically sets the two fluids into motion. The position of the gate was chosen to maximize the duration of the constant-velocity phase, while providing sufficient runout in the ambient fluid to observe the intrusion speed unaffected by internal waves reflected from the endwall of the tank. Sodium chloride was added to water to vary the density between 1.010 and 1.060 $\mathrm{g\,cm}^{-3}$. Stratification was created using the double-bucket method (Oster 1965) and sponge floats were used to fill both sides of the lock gate simultaneously to $H = 20$ cm depth. Water samples were drawn every 2 cm in height from both fluids, and the densities were verified with an Anton-Paar 5000 DMA density meter with an accuracy of 10^{-8} $\mathrm{kg\ m}^{-3}$. Only density profiles with levels of neutral buoyancy deviating less than ± 2 mm from $H/2$ were included.

The channel was illuminated by a vinyl light sheet placed against the back wall. A CCD camera (1390 × 1024 pixel resolution) was positioned normal to, and 5 m away from, the front wall. Sucrose-based food colouring, with a molecular diffusion coefficient approximately one-third that of sodium chloride, was added to the lock-fluid double-bucket system as a passive tracer of density. Images of the current were recorded directly onto a PC via DigiFlow software (Dalziel 2004) at 12 frames s^{-1}. The same software was used to track the horizontal and vertical extent of the dyed intrusion. The attenuation of the light passing through the tank was measured and used via calibration to provide a width-averaged measure of the density. Mixing at the boundaries of the current decreases the dye concentration and therefore the

https://doi.org/10.1017/S0022112009993752 Published online by Cambridge University Press

light attenuation. To provide a conservative estimate of the thickness of the current, we defined the current edges by a 25 % reduction in the light attenuation of the intruding fluid relative to the average initial light attenuation in the lock.

The intrusion thickness was measured at each frame as the horizontal average of the thickness of a 10 cm long section of intrusion, as determined by the vertical extent of the dyed region, centred 7 cm behind the lock gate. Distance–time (x–t) plots of the position of the front of the intrusion were created by projecting the density field onto the horizontal axis at each frame. A linear regression was then fitted to the plot to estimate the constant velocity of the progressing density front (Shin, Dalziel & Linden 2004).

3.2. *Numerical simulations*

Direct numerical simulations of lock releases were conducted in two dimensions for two values of the ambient buoyancy frequency $N_a = 0.5\ \mathrm{s}^{-1}$ and $1.0\ \mathrm{s}^{-1}$, and for eleven equally spaced values of the stratification parameter $S = 0, 0.1, \ldots, 1$.

For an incompressible Boussinesq fluid of uniform viscosity ν in two dimensions (x, z), the governing equations are

$$\nabla \cdot \boldsymbol{u} = 0, \tag{3.1}$$

$$\frac{\mathrm{D}u}{\mathrm{D}t} = -\frac{1}{\rho_0}\frac{\partial P}{\partial x} + \nu\nabla^2 u, \tag{3.2}$$

$$\frac{\mathrm{D}w}{\mathrm{D}t} = -\frac{1}{\rho_0}\frac{\partial P}{\partial z} - \frac{g\rho'}{\rho_0} + \nu\nabla^2 w, \tag{3.3}$$

$$\frac{\mathrm{D}\rho}{\mathrm{D}t} = \frac{\nu}{Sc}\nabla^2\rho, \tag{3.4}$$

where $\boldsymbol{u} = (u, w)$ is the velocity, P is the hydrostatically adjusted pressure, $Sc = \nu/\kappa$, where κ is the molecular diffusivity of salt, is the Schmidt number and ρ' is a perturbation from the average background density.

For the simulations reported here, the kinematic viscosity is $\nu = 0.01\ \mathrm{cm}^2\,\mathrm{s}^{-1}$ and $Sc = 1$. For salt water $Sc \gg 1$ and, although the choice of $Sc = 1$ leads to an overestimation for the diffusivity of salt, this choice is necessary to maintain numerical stability. This is standard practice in these types of calculations and does not appear to lead to significant changes in the dynamics of the flow; see e.g. Hartel, Meiburg & Necker (2000). Mass transfer from the current is determined by the Péclet number $Pe = (N_a h_i^2)/(\kappa)$, where κ is the molecular diffusivity of mass. At high values of $Pe \gg 1$, molecular transport is not important and instead the density of the current changes, if at all, by mixing with the ambient fluid. At high Reynolds numbers, the choice of $Sc = 1$ means that the Péclet number is also large so that the effects of mass diffusion, like those of viscosity, are expected to be small.

A slightly modified version of the open source DNS algorithm Diablo (full details available at http://renaissance.ucsd.edu/fccr/software/Diablo.html) was used to solve the above equations. The code in its current form requires periodic boundary conditions in the streamwise direction, and the flow here is not periodic in the streamwise direction. In order to achieve periodicity and enable a Fourier decomposition of the flow variables in this direction, a domain twice the length of the domain shown in figure 1 was chosen. This allows reflexional symmetry about the vertical midplane in the initial condition (i.e. lock fluid starts in the middle and propagates equally in both horizontal directions). In the vertical direction periodicity

https://doi.org/10.1017/S0022112009993752 Published online by Cambridge University Press

does not occur. Derivatives in this direction were evaluated using centred finite differences with no-slip boundary conditions at the top and bottom boundaries.

A mixed method using third-order, low-storage Runge–Kutta–Wray (RKW3) scheme and a Crank–Nicholson (CN) scheme was used to advance the flow in time with $\Delta t = 0.001$ s. Diffusive terms in the wall-normal direction were treated implicitly, while all other terms were treated explicitly. Uniform grids were selected in all directions.

As with the laboratory experiments, the flow is stationary at $t = 0$. In order to minimize Gibbs phenomena in the streamwise direction, the vertical interfaces that define the lateral boundaries of the lock were smoothed using a hyperbolic tangent profile.

Parameters were chosen so that the Reynolds number, $Re = (N_a h_i^2)/\nu$, based on the intrusion thickness h_i, is sufficiently large (i.e. $> 10^4$) that viscous effects are negligible and the flow exhibits the characteristic features of two-dimensional turbulent gravity currents such as the roll up of Kelvin–Helmholtz billows behind the gravity current head.

The numerical simulations were allowed to progress until the finite length of the domain began to influence the intrusion. In the same manner as in the experiments, the intrusion thickness was estimated at each frame as the horizontal average of a 10 cm section of intrusion thickness centred 7 cm behind the lock gate.

4. Results

Simulations for $N_a = 0.5\,\mathrm{s}^{-1}$ and $N_a = 1\,\mathrm{s}^{-1}$ and experiments for $N_a = 1.47 \pm 0.02\,\mathrm{s}^{-1}$ were conducted over the range of stratification ratios $0 \leqslant S < 1$. An example of the current at various times from the numerical simulations is shown in figure 2 for $S = 0.2$ and $S = 0.8$. A similar series from the experiments at the same dimensionless times is shown in figure 3 for $S = 0.23$ and $S = 0.77$. Ignoring the exaggerated billows in the two-dimensional simulations, which in practice break down as a result of three-dimensional instabilities that are precluded from the calculations, we observe excellent agreement between the experimental and numerical images. The shapes of the simulated intrusions agree well the experimental images, although the front of the intrusion is more ragged at $S = 0.8$ in the experiments. The reduction in the intrusion speed and its increase in thickness as S increases are seen in both the experiments and the simulations. Quantitatively, the experiments and the simulations agree well, even though they are for different values of N_a. This agreement, achieved by non-dimensionalizing time with the ambient buoyancy frequency, supports the dimensional analysis leading to (2.4).

The intrusions taper towards the front similar to those observed for unstratified intrusions (Bolster *et al.* 2008); see also figure 6. There is no evidence of a 'head' typical of gravity currents in unstratified environments. A close inspection of the edges of the stratified intrusions shows some irregular structures. These have not been observed on either gravity currents or unstratified intrusions and are a result of the internal stratification within the intrusion. We will examine them further below.

In order to test the predictions (2.7), (2.9) and (2.12) for the variation of front speed with S, we need to measure how the thickness of the intrusion varies. As observed in figures 2 and 3, the thickness of the intrusion increases with increasing S, while the thicknesses of the backflows decrease. As noted above, the thickness is not uniform in x, and we observe sloping boundaries between the intruding and ambient fluid narrowing towards the front of the intrusion. It is for this reason that

https://doi.org/10.1017/S0022112009993752 Published online by Cambridge University Press

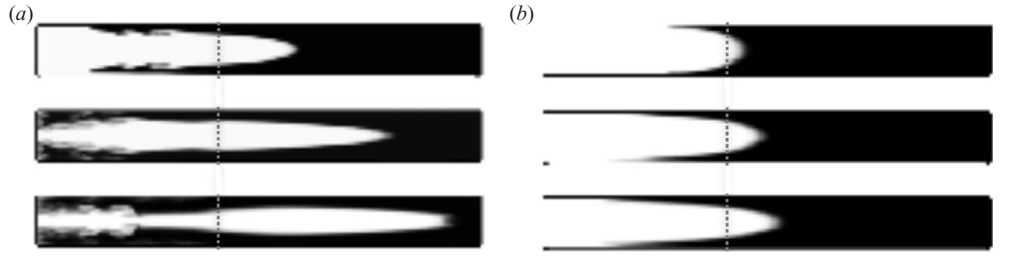


FIGURE 2. Snapshots of the numerical simulations for $S = 0.20$ (a) and $S = 0.80$ (b) for $N_a = 1$ s^{-1} at $N_a t = 10$, 20 and 30. The dotted line denotes the initial position of the gate. The motion of the lock fluid is visualized using a passive tracer.

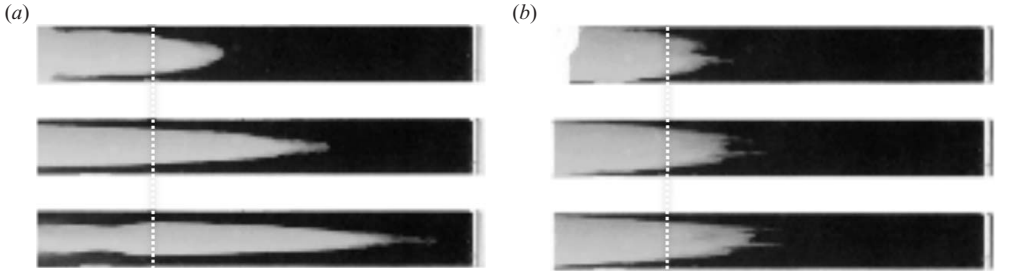


FIGURE 3. Snapshots of the laboratory experiments for $S = 0.23$ (a) and $S = 0.77$ (b) for $N_a = 1.5$ s^{-1} at the same dimensionless times $N_a t = 10$, 20 and 30 as in figure 2. The dotted line denotes the initial position of the gate. The intrusion fluid is visualized with dye.

we chose to measure a representative thickness taken to be the spatial and temporal average thickness of a 10 cm long region centred 7 cm back from the gate position. The consequences of choosing an alternative location for the thickness measure are discussed in § 6.

In Figure 4, we compare the intrusion thickness h_i as a function of S for the laboratory experiments and numerical simulations with the assumed linear variation in current thickness (2.8). At lower values of $S < 0.5$, both the numerical and experimental results agree within the error bounds, which for the simulations are large as a result of the billows referred to above, and they agree well with the linear approximation (2.8). At higher values of S the agreement is not as good: the experimental thicknesses are less than the simulations, and the latter show better agreement with (2.8) over the entire range of stratification ratios.

As in the case of unstratified intrusions into a linearly stratified ambient fluid (Bolster *et al.* 2008), the stratified intrusions were observed to travel at a constant speed after an initial period of acceleration once the lock gate was removed. Figure 5 displays the dimensionless front speed as a function of S. Intrusion speeds measured in the laboratory experiments and numerical simulations agree well over the entire range $0 \leqslant S < 0.8$. As noted in § 2 the bounds for the velocity are given by Bolster *et al.* (2008) for $S = 0$, and by inspection ($U_i = 0$) at $S = 1$. Between these bounds, the available potential energy, and therefore the intrusion velocity, decreases monotonically with increasing S, as observed.

Curves corresponding to the predictions (2.7), (2.9) and (2.12) are given in figure 5. The simplest case, (2.7), in which only the motion of the intrusion itself is included, and which ignores changes in intrusion thickness with S, overpredicts the speed at

https://doi.org/10.1017/S0022112009993752 Published online by Cambridge University Press

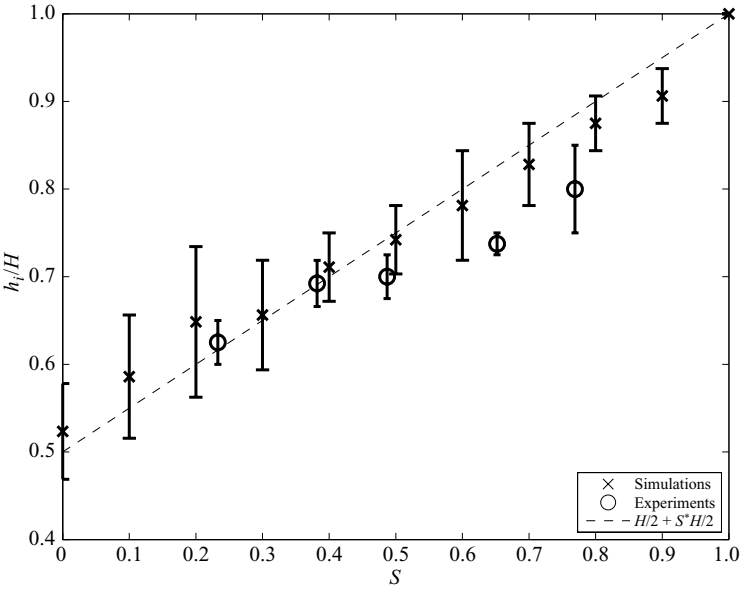


FIGURE 4. A comparison between dimensionless intrusion thickness h_i/H, where H is the total fluid depth, as a function of the stratification ratio S for experiments (circles), simulations (crosses) and the thickness assumed in the energy balance model (2.8) (dashed line). The thickness in the experiments was measured at each time as the 10 cm spatial average of intrusion thickness centred 7 cm behind the lock gate, and the resulting time averages and standard deviations are shown.

all values of $S > 0$. When the variation in intrusion thickness is included in (2.9) the model predictions improve but still overestimate the observed and calculated speeds particularly at large S.

The theoretical estimate (2.12) that includes both the variation in intrusion thickness and the kinetic energy of both the intrusion and the two counterflowing gravity currents, provides the best agreement with the observed and calculated speeds. Agreement between the first-order model and the experimental and numerical results is better than 5 %, over the range $0.3 \leqslant S < 0.9$. Furthermore, the curvature of (2.12) has the opposite sign to the two simpler estimates (2.7) and (2.9), and is consistent with the curvature observed in the data at large S. For values of $S < 0.3$, the data lie between the curves given by (2.9) and (2.12).

5. Role of internal stratification

Compared to unstratified intrusions in a linearly stratified ambient fluid studied by Bolster *et al.* (2008), the presence of stratification in the intruding fluid changes both the shape and the speed of the intrusion. Figure 6 shows a comparison between intrusions for $S = 0$, 0.23 and 0.77. For the unstratified intrusion $S = 0$, the front takes the shape of a classical rounded plug of fluid shape first described by Benjamin (1968). The theoretical shape predicted by Benjamin (1968) for an irrotational gravity current and ignoring any internal flow within the current, which is also a good approximation for the shape of an interfacial intrusion on a sharp density interface (Lowe *et al.* 2002), is superimposed on the unstratified intrusion in figure 6. The rounded front of the intrusion agrees well with this shape, suggesting that there is little relative flow

https://doi.org/10.1017/S0022112009993752 Published online by Cambridge University Press

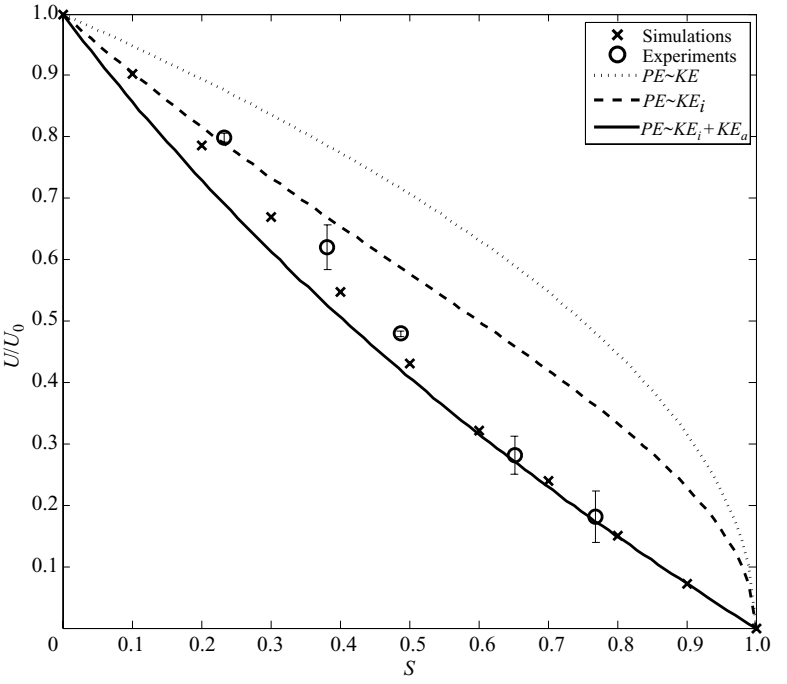


FIGURE 5. A comparison between dimensionless intrusive gravity current speed in the experiments (circles), simulations (crosses) and model predictions (curves) as a function of stratification ratio S. The three models of increasing complexity approximate the variation of U_i with S, directly from the potential energy ((2.7), dotted line), and scaled by a linear increase in current thickness with S ((2.9), dashed line), and incorporating the counterflow ((2.12), solid line). U_0 is taken to be the speed of a well-mixed intrusion $U_0 = 0.125 N_a H$.

within the intrusion. Farther back from the front the top and bottom surfaces of the intrusion continue to slope and the intrusion continues to increase in thickness towards the rear, in contrast to the gravity current.

In addition to increasing in thickness as S increases, stratified intrusions do not exhibit the rounded front observed in the $S = 0$ case. The front is more pointed for the case $S = 0.23$, and shows an almost vertical face with some smaller intrusions of dye fluid for the case $S = 0.77$. The unstratified intrusion flows along the isopycnal surface in the ambient fluid corresponding to its internal density and that isopycnal splits along the top and bottom surfaces of the intrusion. When $S > 0$, this simple splitting of the ambient fluid above and below the intrusion is not possible, because the density stratification within the intrusion implies that a range of the ambient density field is within the density variations within the intrusion.

Figure 7 shows the calculated density contours for stratified intrusions $S = 0.2$ and $S = 0.8$. The contours shown in each case correspond to the full density range within the intrusion and the same isopycnals in the ambient fluid. So, in the $S = 0.2$ case, only isopycnals near the mid-depth of the ambient fluid are marked. In this case, small density inversions occur at the edges of the intrusion as heavier fluid is raised above the intrusion and lighter fluid is pushed below it. These inversions are distinct from the larger-scale billows caused by shear instability on the edges of the intrusion (figure 2). They can be seen in the experimental images of the stratified intrusions in figures 3 and 6, and in the simulations shown in figure 2. These inversions occur

https://doi.org/10.1017/S0022112009993752 Published online by Cambridge University Press

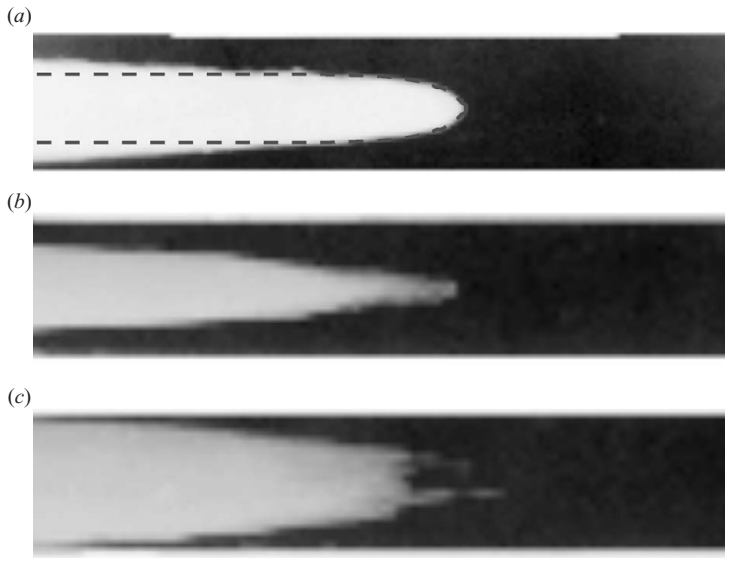


FIGURE 6. A comparison of the front shape in laboratory experiments at $N_a = 1.47 \pm 0.02\,\mathrm{s}^{-1}$ for three different stratification ratios, $S = 0$, 0.23 and 0.77. The presence of stratification within the intrusion generates internal circulation within the intrusion and its thickness increases with increasing S. The shape of an irrotational gravity current given by Benjamin (1968) is superimposed on the unstratified intrusion $S = 0$.

because of the variation of density within the intrusion, because, for example, the density of the mid-depth isopycnal in the ambient, which bifurcates at the intrusion front, is greater than all of the fluid in the upper half of the intrusion.

Distortions of the isopycnal surfaces upstream of the intrusion are also seen in figure 7. As the intrusion forcing is centred about the midplane of the tank, we expect mode 2 waves to be strongly forced. Bolster *et al.* (2008) determined that well-mixed intrusions in a linearly stratified ambient fluid travel at speeds subcritical to mode 1 and mode 2 waves. The introduction of stratification in the intruding fluid reduces its speed, and indeed, the spreading apart of the isopycnals above and below the midplane in the ambient fluid upstream of the current is consistent with the presence of a mode 2 disturbance.

For the more stratified intrusion $S = 0.8$, the adjustment of the isopycnals is less than for the $S = 0.2$ case. There is some compression of the intrusion isopycnals near the front of the intrusion and an upstream disturbance in the form of a mode 2 wave. There is an adjustment region ahead of the intrusion front. However, no evidence of overturning or statically unstable regions is observed on the images in figures 2 and 3. It appears that dye distortions remain after the instabilities that generated them have decayed.

The compression of the isopycnals within the intrusion and also in the counterflowing gravity currents above and below the intrusion change the stratification in those flows. Figure 8 shows vertical profiles of buoyancy frequency N at a location ahead of the original lock gate position (see figure 7) at $N_a t = 20$. Also shown in the figure are the values of the initial buoyancy frequencies in the intrusion and the ambient fluid, N_i and N_a, respectively. In both cases the stratification within the intrusions remains linear and increases from its initial value to a constant value of N between N_i and N_a. The ambient fluid in the counterflowing gravity currents also

https://doi.org/10.1017/S0022112009993752 Published online by Cambridge University Press

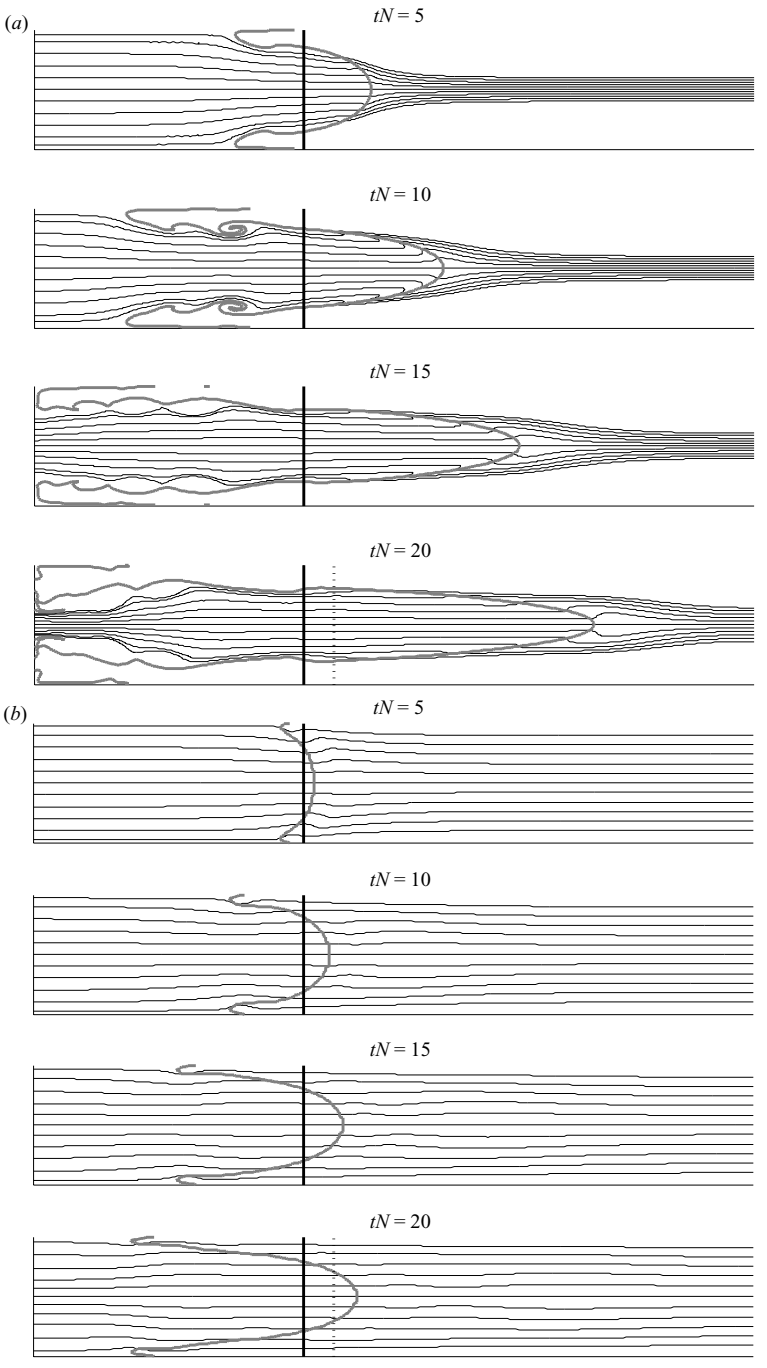


FIGURE 7. Snapshots of the density contours for $S = 0.20$ and $S = 0.80$ ($N_a = 1\ \mathrm{s}^{-1}$) at $N_a t = 5, 10, 15$ and 20, calculated from the simulation data. The black lines denote density contours evenly spaced across the entire range of intrusion densities, and the corresponding isopycnals in the ambient fluid. The grey lines denote the boundary between the intrusive and the ambient fluids, the black line denotes the initial position of the gate and the dashed black line denotes the vertical transect described in figure 8. Note the pronounced step in the density contours at the transition between the two fluids in the more energetic $S = 0.2$ case, the horizontal gradients in density created within and ahead of the intrusion, and finally the adjustment of the upstream ambient stratification.

https://doi.org/10.1017/S0022112009993752 Published online by Cambridge University Press

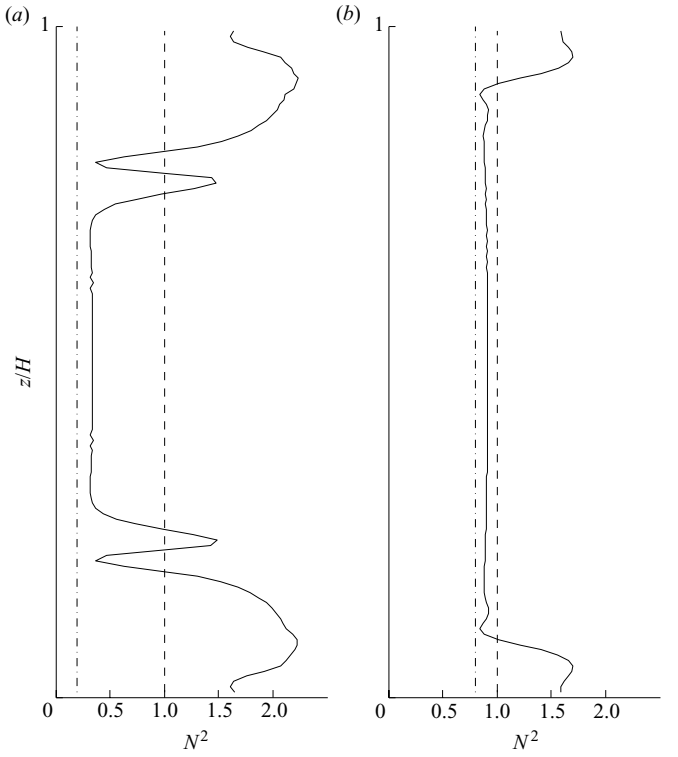


FIGURE 8. Vertical transects of the buoyancy frequency, for $S = 0.2$ (a) and $S = 0.8$ (b), taken 5 cm into the ambient fluid from the gate position at $N_a t = 20$ (see figure 7). The dash-dotted line and the dashed lines denote the initial buoyancy frequency profiles of the intruding and ambient fluids, N_i and N_a, respectively. The solid line is the instantaneous buoyancy frequency as a function of height at the given x location. Note that the buoyancy frequency of the intruding fluid (closer to the mid-depth) reaches an intermediate value between the N_i and N_a, while the counterflowing boundary gravity currents also display an increased buoyancy frequency.

increases in stratification as the fluid above and below the intrusion is compressed vertically. The edges of the intrusion are marked by rapid increases and decreases in N associated with the local distortion of the density field.

The horizontal density gradients that occur within the intrusion as a result of the compression of the isopycnals towards the front generate internal flow. Vorticity is produced by the baroclinic generation term $\nabla p \times \nabla \rho$, and the sign of this term is such as to produce positive vorticity in the upper half of the intrusion and negative vorticity in the lower half. This produces a dipole-like flow towards the front of the intrusion along the middle and return flow along the top and bottom boundaries. This internal flow is consistent with an elongation of the front of the intrusion from the irrotational shape observed in the unstratified case (figure 6), and the return flow is consistent with the distortion of the isopycnals observed for the case $S = 0.2$ (figure 7).

6. Discussion and conclusions

This paper examines the mutual adjustment of two stratified fluids instantaneously brought into contact in a channel by the removal of a vertical barrier. The fluids

https://doi.org/10.1017/S0022112009993752 Published online by Cambridge University Press

are stratified with linear variations of density with depth, but with different vertical density gradients. We have restricted attention to the case where the two fluids have the same mean densities which occur at the same depth, in this case the mid-depth of the channel. In this case the centres of mass of the two fluids are at the same height, and the fluids have no tendency to flow one under the other. The motion is vertically symmetrical about the mid-depth of the tank with the less stratified fluid flowing into the more strongly stratified fluid as an intrusion centred at the mid-depth. The more stratified fluid flows in the opposite direction as two stratified gravity currents: one above the intrusion along the upper boundary of the fluid and one below along the lower boundary.

This configuration has two limits. The first is when one of the fluids is unstratified, in which case the flow is that of an unstratified intrusion propagating along the mid-depth of a stratified fluid. This case has been studied previously (Bolster *et al.* 2008) and its properties are known. The other limiting case is when the density gradients of the two fluids are the same. In this case, the two fluids are indistinguishable and nothing happens.

Through lock-exchange laboratory experiments and two-dimensional numerical simulations we have examined the behaviour of the system between these two limits in terms of the stratification ratio $S \equiv N_i^2/N_a^2$. The unstratified intrusion corresponds to $S = 0$ and the two identical fluids to $S = 1$. In all cases $S < 1$ we observe that the flow takes the form of an intrusion of the less stratified fluid (N_i) into the more strongly stratified fluid. This intrusion propagates along the mid-depth of the channel and two counterflowing gravity currents flow above and below the intrusion.

One objective was to predict the speed of the intrusion as a function of S. We observed that the intrusion travelled at a constant speed, which decreased as a function of increasing S, and found good agreement between the measured speed in the experiments and that calculated in the simulations. We developed a model for the exchange flow that assumes that the available potential energy of the initial configuration is converted at a constant rate into the kinetic energy of the intrusion and the gravity currents. As expected, the model also predicted a reduction in speed with S and gave reasonably good agreement with the experimental and numerical data (figure 5).

The model relies on an estimate of the thickness of the intrusion and the counterflowing gravity currents. We observed that the intrusion thickness increased with S, which is to be expected as the extreme densities within the intrusion correspond to a wider region about the mid-depth of the ambient fluid as S increases. We approximated this increase as a linear function of S, which is consistent with the width of the corresponding region in the ambient fluid, and found reasonable agreement with the data (figure 4).

The sloping boundaries of the intrusions introduce variability to the measurements of the current thickness as a function of horizontal location. Measurements of the current thickness within the lock are at a thicker part of the current, and therefore likely to be an overestimate. To examine the sensitivity to the choice of the horizontal position at which the thickness is measured, we reduce the assumed intrusion thickness (2.8) by a factor $c < 1$, and write the intrusion thickness as

$$h_i = c\frac{H}{2}(1 + S). \tag{6.1}$$

https://doi.org/10.1017/S0022112009993752 Published online by Cambridge University Press

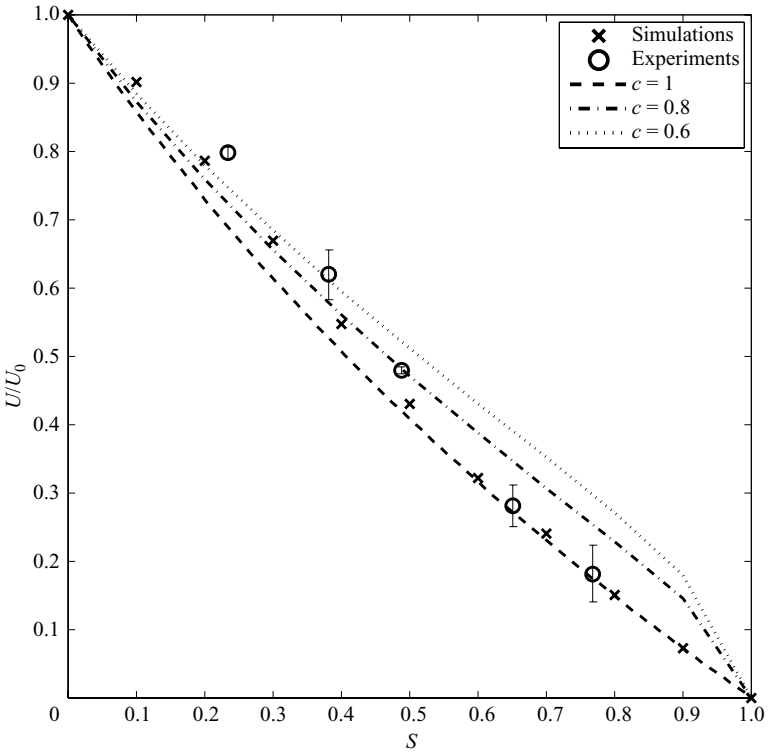


FIGURE 9. A comparison between modelled dimensionless intrusive gravity current speed presented in figure 5 (dashed line) and speeds predicted based upon a reduced intrusion thicknesses. Energy balance model predictions of intrusion speed where the well-mixed intrusion thickness is $0.5H$, $0.4H$ and $0.3H$ ($c = 0.8$ and 0.6) are shown by dashed, dash-dotted and dotted lines, respectively. Note that relatively large reductions in the thickness of the intrusion result in a less significant increase in predicted speed, and that at lower values of S, this reduced thickness provides an improved fit to the numerical and laboratory data.

By the same energy argument as presented in (2.12), we arrive at an expression for the dependence of the velocity on S

$$f(S) \sim \frac{(1-S)}{(1+S)} \frac{\left(1-\frac{c}{2}(1-S)\right)}{\left(1-\frac{c}{2}\right)}. \tag{6.2}$$

The modelled speeds for various values of c are plotted in figure 9. Compared with the case presented in § 4 ($c = 1$), the speeds predicted using a reduced thickness are faster over the range of intermediate stratification ratios as c decreases. At lower stratification ratios, $S < 0.5$, the use of a reduced current thickness predicts intrusion speeds in closer agreement with experimental and numerical observations. The boundaries of low S intrusions are more sloped (figures 3 and 6), and so are better represented by a reduced thickness than that used in § 4, while intrusions at higher stratification ratios $S > 0.5$ are better described by the full-thickness energy balance models. In any event these changes are small and the sensitivity to the exact value chosen for the intrusion thickness is small: a reduction of the assumed current thickness by 40 % results in a maximum change in the predicted speed of less than

https://doi.org/10.1017/S0022112009993752 Published online by Cambridge University Press

15 %, indicating that the model is relatively robust to inaccuracies in the assumed current thickness.

The agreement between this energy-conserving model and the experiments and simulations is consistent with previous work on interfacial intrusions (Cheong *et al.* 2006) and unstratified intrusions in a linearly stratified ambient fluid (Bolster *et al.* 2008). This conversion of available potential energy to kinetic energy of the intrusion and ambient flows ignores dissipative processes such as turbulence and mixing (and viscosity, but this is small at the high Reynolds numbers we are considering). It also ignores energy escaping into upstream waves, which are undoubtedly present in these flows. We conclude, that while these processes occur, their impact on the overall energetics is small and can be ignored to first order.

As noted in § 5, internal waves are present in the stratified ambient fluid. They occur both upstream of the intrusions which are subcritical to, at least, long waves of vertical modes 1 and 2. Waves are also present in the ambient fluid behind the front of the intrusion. It is also likely that there are internal waves within the stratified intrusion itself, although they have not been clearly identified. The effects of these waves need further study, which is also the case for unstratified gravity currents (Maxworthy *et al.* 2002) and intrusions (Bolster *et al.* 2008). As in the present study, the speed of the gravity current and intrusion could be predicted while ignoring the internal waves entirely. On the other hand, recent experiments by Munroe *et al.* (2009) show quite different behaviour for unstratified intrusions which appears to result from the influence of internal waves reflected from the back of the lock, causing little evidence of a constant-velocity phase.

The model also ignores the internal circulation that results from the internal stratification in the intrusion. We observe that baroclinic generation of vorticity generates a dipolar internal flow that distorts the isopycnals within the intrusion and changes the shape from the unstratified intrusion which is well represented by an irrotational interior. We also observe that adjustment of the isopycnals leads to small regions of static instability along the top and bottom of the intrusions. All of these features are excluded from the bulk model that we have presented. Consequently, they seem to play only a secondary role in the bulk adjustment process of two stratified fluids.

Finally, we note that in the case $S \to 1$, the interchange between the two fluids decreases and the flows become weak. Although it may seem that this limit is of little practical relevance as everything evolves very slowly relative to the smaller values of S, one should be cautious before disregarding it. In certain practical cases it has been shown that slow exchange flows are the source of unexpected coastal pollutants (Bolster, Tartakovsky & Dentz 2007).

We are very pleased to be able to contribute to this special issue for Steve Davis and mark his outstanding contributions to fluid mechanics and the *Journal*. This research was supported by the National Science Foundation grant CTS 0756396.

REFERENCES

Amen, R. & Maxworthy, T. 1980 The gravitational collapse of a mixed region into a linearly stratified fluid. *J. Fluid Mech.* **96** (1), 65–80.

Benjamin, T. B. 1968 Gravity currents and related phenomena. *J. Fluid Mech.* **31** (2), 209–248.

Bolster, D. T., Hang, A. & Linden, P. F. 2008 The front speed of intrusions into a continuously stratified medium. *J. Fluid Mech.* **594**, 369–377.

https://doi.org/10.1017/S0022112009993752 Published online by Cambridge University Press

Bolster, D. T., Tartakovsky, D. M. & Dentz, M. 2007 Analytical models of contaminant transport in coastal aquifers. *Adv. Water Resour.* **30**, 1962–1972.

Cheong, H. B., Kuenen, J. J. P. & Linden, P. F. 2006 The front speed of intrusive gravity currents. *J. Fluid Mech.* **552**, 1–11.

Dalziel, S. B. 2004 *Digiflow Manual*, 1st edn. Dalziel Research Partners.

Faust, K. M. & Plate, E. J. 1984 Experimental investigations of intrusive gravity currents entering stably stratified fluids. *J. Hydraul. Res.* **22** (5), 315–325.

Hartel, C., Meiburg, E. & Necker, F. 2000 Analysis and direct numerical simulation of the flow at a gravity-current head. Part 1. Flow topology and front speed for slip and no-slip boundaries. *J. Fluid Mech.* **418**, 189–212.

Keulegan 1958 The motion of saline fronts in still water. *Natl Bur. Stand. Rep.* **5813**.

Lowe, R. J., Linden, P. F. & Rottman, J. W. 2002 A laboratory study of the velocity structure in an intrusive gravity current. *J. Fluid Mech.* **456**, 33–48.

Maxworthy, T., Leilich, J., Simpson, J. E. & Meiburg, E. H. 2002 The propagation of a gravity current into a linearly stratified fluid. *J. Fluid Mech.* **453**, 371–394.

Munroe, J. R., Voegeli, C., Sutherland, B. R., Birman, V. & Meiburg, E. H. 2009 Intrusive gravity currents from finite length locks in a uniformly stratified fluid. *J. Fluid Mech.* **635**, 245–273.

Nokes, R. I., Davidson, M. J., Stepien, C. A., Veale, W. B. & Oliver, R. L. 2008 The front condition for intrusive gravity currents. *J. Hydraul. Res.* **46** (6), 788–801.

Oster, G. 1965 Density gradients. *Sci. Am.* **213**, 70.

Rottman, J. W. & Simpson, J. E. 1983 Gravity currents produced by instantaneous release of a heavy fluid in a rectangular channel. *J. Fluid Mech.* **135**, 95–110.

Shin, J. O., Dalziel, S. B. & Linden, P. F. 2004 Gravity currents produced by lock exchange. *J. Fluid Mech.* **521**, 1–34.

Simpson, J. E. 1997 *Gravity Currents*, 2nd edn. Cambridge University Press.

Ungarish, M. 2005 Intrusive gravity currents in a stratified ambient: shallow-water theory and numerical results. *J. Fluid Mech.* **535**, 287–323.

https://doi.org/10.1017/S0022112009993752 Published online by Cambridge University Press